

# Measurement of secondary cosmic ray intensity at Regener-Pfotzer height using low-cost weather balloons and its correlation with solar activity

Ritabrata Sarkar<sup>a,\*</sup>, Sandip K. Chakrabarti<sup>b,a</sup>, Partha Sarathi Pal<sup>a</sup>,  
 Debashis Bhowmick<sup>a</sup>, Arnab Bhattacharya<sup>a</sup>

<sup>a</sup>*Indian Centre for Space Physics, 43 Chalantika, Garia Station Rd., Kolkata 700084,  
 West Bengal, India*

<sup>b</sup>*S.N. Bose National Centre for Basic Sciences, JD Block, Salt Lake, Kolkata 700097,  
 West Bengal, India*

---

## Abstract

Cosmic ray flux in our planetary system is primarily modulated by solar activity. Radiation effects of cosmic rays on the Earth strongly depend on latitude due to the variation of the geomagnetic field strength. To study these effects we carried out a series of measurements of the radiation characteristics in the atmosphere due to cosmic rays from various places (geomagnetic latitude:  $\sim 14.50^\circ$  N) in West Bengal, India, located near the Tropic of Cancer, for several years (2012-2016) particularly covering the solar maximum in the 24th solar cycle. We present low energy (15 – 140 keV) secondary radiation measurement results extending from the ground till the near space ( $\sim 40$  km) using a scintillator detector on board rubber weather balloons. We also concentrate on the cosmic ray intensity at the Regener-Pfotzer maxima and find a strong anti-correlation between this intensity and the solar activity even at low geomagnetic latitudes.

*Keywords:* Cosmic ray, Regener-Pfotzer height, Solar activity, X-ray detector, Weather balloon-borne mission

*PACS:* 94.20.wq, 94.05.Sd, 95.55.-n, 95.55.Ka, 96.60.Q

---

\*Corresponding author

*Email addresses:* ritabrata.s@gmail.com (Ritabrata Sarkar), sandipchakrabarti9@gmail.com (Sandip K. Chakrabarti), parthasarathi.pal@gmail.com (Partha Sarathi Pal), debashisbhowmick@gmail.com (Debashis Bhowmick), arnabseacom@yahoo.com (Arnab Bhattacharya)

---

## 1. Introduction

Interaction of primary Cosmic Rays (CR) with the atmospheric gas nuclei produces secondary particles and radiations which can be measured in situ by radiation detectors giving rise to an indirect measurement of the primary. This is the dominating radiation in the upper atmosphere below an altitude of about 60 km. At heights close to the ground (say, below  $\sim 2$  km), the radiation field is dominated by terrestrial radioactive sources ([Bazilevskaya et al., 2000](#)).

The secondary CR cascade starting at the upper atmosphere gradually gets intensified at lower heights and have a maximum radiation at a height about 15–20 km depending on the latitude ([Bazilevskaya et al., 2000](#)), where the generation of the secondary radiation is balanced by the loss effects. This effect was observed by direct measurement of ionization at various heights in the atmosphere almost a century ago by Erich Regener and George Pfozter ([Pfozter, 1936](#); [Regener, 1933](#); [Regener and Pfozter, 1935](#)). This point of maximum radiation is now called the Regener-Pfozter maximum (RP-max) and below this point the secondary radiation intensity is gradually reduced due to absorption and decay processes ([Gaisser, 1990](#); [Grieder, 2001](#)).

The intensity of the primary CR, on the other hand, depends on the strength and spatial distribution of the Earth’s magnetic field ([Störmer, 1955](#)). This is a highly dynamical system which is influenced by the solar wind and the interaction between the terrestrial and Interplanetary Magnetic Fields (IMF). Solar Energetic Particles (SEP) generated in the solar atmosphere due to various explosive processes can significantly affect the space environment and produce hazardous radiation effects disturbing the satellite operations, manned or robotic missions in the low-earth orbits often affecting the crews and passengers in commercial aircrafts ([Radiation exposure prediction, 2016](#); [Miroshnichenko, 2003](#)).

Strong perturbations of the geomagnetic field due to the earthward directed SEPs can culminate in geomagnetic storms due to large transfer of solar wind energy to geomagnetic fields. This can significantly change the current, plasma and the field intensity as well as its structure. The intense geomagnetic storms can affect geomagnetic shielding and thus affect the distribution of the planetary CR ([Dorman et al., 1971](#)). Due to this shielding effect, the location and the amount of radiation at the RP-max and in the

stratosphere were found to depend on the geomagnetic latitude (Bazilevskaya and Svirzevskaya, 1998; Golenkov et al., 1977, 1990; Shea et al., 1987). This secondary radiation also varies with solar activity (Charakhchyan et al., 1975, 1979) but this variation is more prominent at higher latitudes and has minimal effect at the low-latitude locations where the geomagnetic rigidity exceeds 10 GV. Results reported in the present paper are performed in this low-latitude region ( $\sim 14.5^\circ$  N).

In situ measurements of the atmospheric parameters through various heights using balloons and aircrafts is a very old subject of interest. Many attempts have been made to measure electrical measurements in the atmosphere (Nicoll, 2012) and to measure radiation levels at various altitudes using radiosonde, mainly at mid and high-latitudes (e.g., Hatakka et al., 2000, in Finland) (Bazilevskaya and Svirzevskaya, 1998, in Russia) (Harrison et al., 2014, in UK) (Yaniv et al., 2016, in Israel). However, the vertical profile of the atmospheric radioactivity data at low geomagnetic latitude around the Tropic of Cancer is not available except in one or two stray cases (e.g., Li et al., 2007, measured in Hong Kong sky). Thus our measurement is expected to extend the study to a wider range of latitudes.

## 2. Mission description

In order to measure secondary radiation due to the CR interaction with atmospheric matter, Indian Centre for Space Physics (ICSP), Kolkata, India has been launching a ‘Dignity’ series of Missions on a regular basis. In these experiments, very light weight payloads (under 2 – 3 kg category) are launched into the atmosphere on board rubber weather balloons which can attain a height of about 40 km. The main instrument used in these missions is a scintillator detector for the detection of X-rays. The details of the detector is given in §3. The payload consists of several other ancillary equipments, such as: Global Positioning System (GPS) unit for the location and altitude measurement; payload Attitude and Heading Reference System (AHRS) using micro electro-mechanical Inertia Measurement Units (IMU) to measure the payload attitude; other sensors for measuring payload’s internal and external temperature and atmospheric pressure; optical video camera unit for the recording of overall mission performance. A general overview of these missions can be found in more detail in Chakrabarti et al. (2014, 2017).

The main detector unit along with its electronic readout system, data storage system, power supply and other ancillary equipments are housed

inside a polystyrene (thermocool) box to give the instruments a shielding from extremely low temperature environment during the entire flight path and also to protect the components from mechanical shock during the landing of the payloads. The payload box is generally cylindrical shaped with overall height of  $\sim 36$  cm and diameter 46 cm. The cylindrical shape of the payload box was adopted in order to reduce the drag effects.

While ICSP is engaged in various near space experiments specifically measuring X-rays from compact objects, several missions were dedicated to measure cosmic ray intensity and spectrum for several years to collect the data on the nature of secondary CR and to study its seasonal or yearly variations under diverse solar conditions. Depending on the tropospheric and stratospheric wind condition, which defines the course of the payload, we launch the payloads from specific places during specific times in the year. In Table 1 the details of mission launch timings and positions concerning this current work are given.

Table 1: Mission timing and positions reported in this paper. The actual mission number in the Dignity series is mentioned within the parenthesis along with the mission index used in this paper.

Mission index.	Date	Launch time (UT)	Landing time (UT)	Launch location <sup>a</sup> (Lat, Lon)
1(D29)	04-06-2012	03:30:19	07:11:26	Bhaluka (23.35N, 88.40E)
2(D45)	24-10-2013	05:46:25	08:35:50	Suri (23.91N, 87.52E)
3(D48)	06-11-2013	04:09:57	07:01:57	Kulti (23.73N, 86.84E)
4(D50)	17-11-2013	04:28:30	07:44:47	Kulti (23.73N, 86.84E)
5(D52)	17-11-2013	19:49:09	01:50:27 <sup>b</sup>	Kulti (23.73N, 86.84E)
6(D57)	17-05-2014	03:48:39	08:26:50	Bolpur (23.67N, 87.69E)
7(D59)	19-05-2014	05:32:47	14:08:00	Bolpur (23.67N, 87.69E)
8(D79)	17-05-2015	04:49:09	07:41:00	Muluk (23.65N, 87.71E)
9(D87)	21-11-2015	04:52:33	07:52:04	Muluk (23.65N, 87.71E)
10(D90)	09-05-2016	04:08:24	08:23:49	Muluk (23.65N, 87.71E)
11(D94)	13-05-2016	04:24:22	08:51:24	Muluk (23.65N, 87.71E)
12(D98)	17-10-2016	03:53:07	06:46:01	Muluk (23.65N, 87.71E)

<sup>a</sup>W.B., India.

<sup>b</sup>Next day.

### 3. Detector description

The scintillator detector used to detect the secondary CR radiation is made of a single NaI(Tl) cylindrical crystal of 2" diameter and 2" thick. This crystal is mounted on a compatible Photo-Multiplier Tube (PMT) of similar diameter and hermetically sealed in an aluminum housing. The whole

integrated detector assembly (crystal + PMT) (model name Bicron Monoline 2M2/2, hereafter B2 detector) is a product of Saint-Gobain Crystals ([Saint-Gobain Crystals, 2016](#)). The front-end electronics system concerning the analog pulse amplification, shaping etc. and the digital electronics part for the digital pulse processing and event storing were designed and fabricated in our laboratory according to the mission requirements. A schematic drawing of the detector fitted with the collimator and the readout system is shown in Figure 1. Though a collimator is not needed in a CR measurement, we kept it for studies of energetic sources. So CR measurements are bi-products of such measurements.

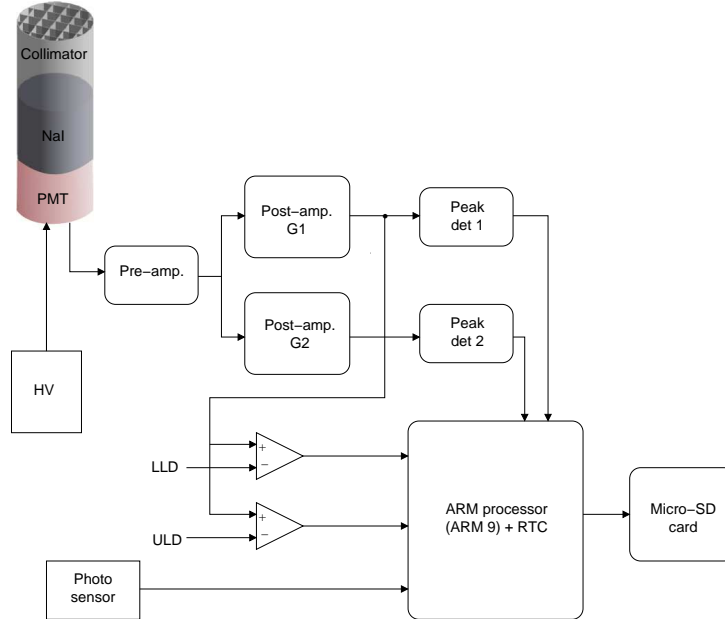


Figure 1: Schematic diagram of the scintillator detector and the event readout system comprising  $2'' \times 2''$  NaI crystal fitted with a  $10^\circ$  FoV lead collimator.

The lower limit of the operating energy range of the detector is defined by the thickness of the detector housing along with the PMT bias voltage and the threshold in the discriminator. The window of the detector is made of 0.5 mm thick aluminum which permits about 30% X-ray at 15 keV. Also the extra-terrestrial X-rays below this limit get absorbed in the residual atmosphere corresponding to the maximum attainable height. The upper limit of the energy range is about  $\sim 5$  MeV as recommended by the detector manufacturer. But due to our science objectives we are more concerned of the

lower energy data requiring better energy resolution in this region. To fulfill this purpose we used two post-amplifiers with different gain settings in the analogue pulse processing part: one (G1) dealing the events in the energy range about 15 – 140 keV and the other (G2) working in the range about 0.1 – 2 MeV. The pulses from the two amplifiers are shaped and converted to digital signal to be stored in a memory card. Two different trigger circuits are dedicated for the trigger generation in two energy ranges.

Collimators made by 0.5 mm thick lead sheets are used to reduce background radiation counts. This is particularly useful for observation of specific sources which we observe along the way. The same lead sheet is also used to shield the detector from radiation entering from sides. Since the lead sheet is capable of blocking  $\sim 100$  keV radiations, above 100 keV, the collimators do not function. Thus we concentrate on the radiations below 60 – 70 keV for our purpose. In case any mission has a different collimator configuration, we normalize all of them using a reference detector.

#### 4. Data analysis

The detectors are provided by collimators of 0.5 mm thick lead with various field of view specific to the Mission. The cylindrical side of the detector is shielded by lead sheet of same thickness. This lead shielding essentially can provide  $\sim 95\%$  blocking of photons up to 100 keV but due to the absorption line at 88 keV and  $K_\alpha$  emission at 75 keV, this collimator effectively blocks up to 60 keV. This defines the upper limit for the energy consideration of our analysis. We restrict the lower energy limit to 25 keV to avoid the noise from the detector at lower energies.

The shielding cannot block high energy photons and these photons pass through the detector crystal to deposit their energy producing new counts. Since the high energy photons are more likely to deposit partial energy (in Compton scattering or pair production) and we do not have any veto detector to discriminate these partial depositions, the detector counts could be contaminated by such photons. So, we do not use photon counts in this range in determining the temporal variation.

##### 4.1. Count normalization

Since the same detector has been used for several years, we have been particularly careful to ensure that the variation of the efficiency of the detector over the years due to bias voltage change or gain shift are corrected for. Also

different configurations of the collimator were used during different missions. Due to these facts, the detector radiation counts need to be normalized with appropriate solid angle.

The radiation counts ( $C_d$ ) obtained by the detector have two components in the energy range under consideration: (i) Number of photons entered into the detector through the FoV ( $C_f$ ) of the collimator and deposited its full energy. This depends on the FoV of the collimator. (ii) Number of high energy photons ( $C_p$ ) entered into the detector through all directions and deposited partial energy into it. This depends on the matter distribution of the detector construction. So we have,

$$C_d = C_f + C_p. \quad (1)$$

To separate full and partial energy deposition counts we take the help of a reference detector which is capable of separating only the number of full energy depositing photons ( $C_{d,r}^m$ ; here d - used for detected photons, r - for reference detector and m - for an altitude of minimum count explained in the following paragraph). This reference detector is a phoswich detector using 3 mm thick NaI and 25 mm thick CsI scintillator crystals of 11.6 cm diameter in combination with a single PMT for signal readout. Thus by operating both the detectors (B2 and the reference detector) under the same conditions number of photons can be calculated with full energy deposition in the B2 detector from the detector characteristics (area, quantum efficiency, FoV) of both the detectors.

To normalize the counts across the missions, we make an assumption that the minimum photon counts due to CR at about 1 km above the ground remains more or less the same for all the missions. This is quite evident in the plot shown in Figure 3. Thus the full energy deposition counts in the B2 detector at the Height of Minimum CR (HMCR) may be calculated as,

$$C_f^m = C_{d,r}^m \frac{A_f}{A_r} \frac{Q}{Q_r} \frac{\Omega}{\Omega_r} \quad (2)$$

and corresponding partial energy deposition counts are,

$$C_p^m = C_d^m - C_f^m, \quad (3)$$

where,  $C_d^m$  is the overall counts detected at HMCR in the mission,  $Q$  and  $Q_r$  are the quantum efficiency of B2 and reference detector in the specified energy,  $\Omega$  and  $\Omega_r$  are the solid angle subtended by the FoV of the collimator

of the two detectors,  $A_f$  and  $A_r$  are the surface area of the detectors window with collimator opening.  $C_{d,r}^m$  can be obtained from a mission with the phoswich detector on board the payload.

From the ratio of the partial and full energy deposition counts at HMCR we can calculate the full  $C_f^p$  and partial  $C_p^p$  energy deposition counts at the RP-height.

$$C_f^p = \frac{C_f^m C_d^p}{C_d^m}, \quad (4)$$

$$C_p^p = C_d^p - C_f^p. \quad (5)$$

The secondary cosmic gamma-ray in the atmosphere depends on the zenith angle or tilt angle of the detector  $\theta_t$  (Shönfelder et al., 1997). Moreover, this  $\theta_t$  dependence again is a function of the altitude as shown in Bazilevskaya and Svirzevskaya (1998). So an index of angle dependence  $h$  is needed in the calculation to incorporate this function. Using the above values, the normalized photon counts at the RP-max can be calculated as,

$$C_n^p = \frac{C_f^p}{QA_f \Omega (\cos \theta_t)^h} + \frac{C_p^p}{QA_a 4\pi} \quad (6)$$

where,  $A_a$  is the overall surface area of the crystal in B2 since high energy photons can enter into the detector from the whole  $4\pi$  solid angle. The effect of the zenith angle from the vertical axis has been taken care by the  $(\cos \theta_t)^h$  term. The unit of this normalized counts is *photons/s/cm<sup>2</sup>/sr*. However, for practical purpose, in the subsequent calculation we have considered the omni-directional counts in unit of *photons/s/cm<sup>2</sup>*.

#### 4.2. Height of Regener-Pfotzer maximum

The Regener-Pfotzer height (RP-height) at the region close to the launching site is estimated by first extracting the average count rate over 100 m height, then a running average of these count rates is taken at different heights to smooth the curve. Next a cubic spline is fitted to determine the position of the maximum count for the RP-max height and corresponding count rate as the Regener-Pfotzer count. It is to be noted that our flights laterally move by a distance of about 20 – 30 km by the time RP-height is reached. So there is negligible influence of variation of latitude between the launching and RP-height coordinates.



## 5. Results and discussions

### 5.1. Geomagnetic latitude effect

All the experiments under consideration of this work were conducted near the Tropic of Cancer as can be seen from Table 1. It is well known that there is a strong dependence of the RP-height with geomagnetic latitude due the variation of cut-off rigidity of the primary cosmic rays entering into the atmosphere (Bazilevskaya and Svirzevskaya, 1998). The average RP-height found in this work is  $15.0 \pm 0.32$  km. The corresponding atmospheric depth is calculated as  $122.70 \pm 6.33$  g/cm<sup>2</sup> considering the atmospheric depth and altitude relation for standard atmosphere as given in Bazilevskaya et al. (2000). The geomagnetic rigidity cut-off at this latitude is 15.6 GV, calculated according to Bobik et al. (2006) using the web based calculator (Geomagsphere.org, 2016). The dependence of the RP-height in terms of atmospheric depth  $p$  with the geomagnetic rigidity cut-off  $R_c$  is shown in Figure 2. Our data in a restricted energy range is represented by a filled square and the data points obtained from Geiger-Müller counters for other latitudes are taken from Bazilevskaya and Svirzevskaya (1998) and Li et al. (2007). Li et al. (2007) used the following empirical formula to fit data:

$$p = 42 R_c^{0.35}, \quad (7)$$

shown by the curve in Figure 2.

Apart from the difference in energy ranges in consideration, unlike these results, our result is by far in the region closest to the geomagnetic equator where the behaviour could be different. Because of these, we believe that our result is not actually falling on the curve proposed by Li et al. (2007).

### 5.2. Ground data comparison

Radiation counts at the ground or sea level mainly depends on the local abundance of radioactive materials and radioactivity of the aerosols at that place (Ageshin et al., 1981). Radiation counts at the lower atmosphere also depends on the seasonal variation and local weather effects like rain, temperature and its distribution etc. In Figure 3 we plot the ground radiation counts for different missions where the data points for the same locations are grouped in the Figure. The ground radiation and local effects gradually vanish with altitude in 1 – 2 km and secondary radiation due to CR starts to dominate. So there is a local minimum in the radiation count profile at

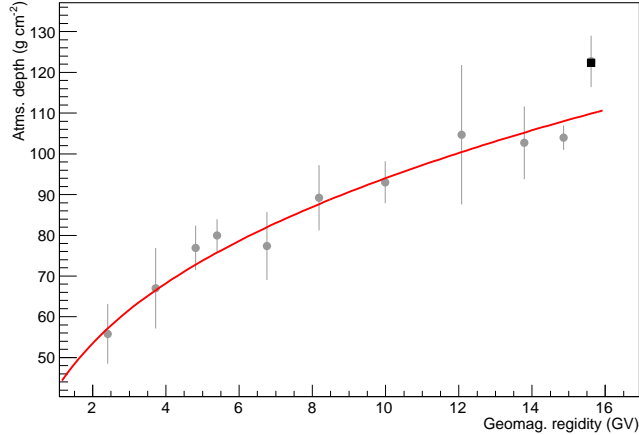


Figure 2: Atmospheric depth at Regener-Pfotzer height vs. geomagnetic rigidity at various locations. The result of the location of current study using a scintillator detector in a narrow energy band is shown with the black square. Other results use Geiger-Müller counters of unrestricted energy band and the curve corresponds to an empirical fit to these results.

that height. The count at the minimum is more or less the same as evident from the same Figure.

### 5.3. Vertical profile of secondary radioactivity

The vertical profile of radioactivity in atmosphere is shown in Figure 4, where the normalized radiation count rates per detector area are plotted in 100 m intervals along with the running average presented by the thick lines. In general, the ground radioactivity and the total count decrease sharply up to about 1 km due to absorption of the ground radiation. The total count starts to increase up to the RP-height due to the increase in secondary radiation for CR interaction in atmosphere and decrease in absorption. Beyond the RP-max the counts decrease due to reduced interaction probability of the CR particles in thinner atmosphere.

To demonstrate variation in the atmospheric radiation profile for different solar conditions, we considered two data sets from two different missions during different phases of solar activity. The atmospheric radioactivity at higher altitudes distinctly shows lower counts for the mission during the solar maxima (October, 2013; Serial No. 2) compared to the data during (May, 2016; Serial No. 11) when the solar maximum is over. Similar type of

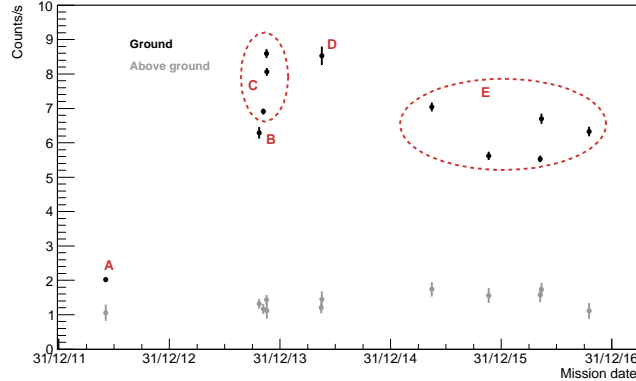


Figure 3: Ground counts (black) and minimum counts above ground (gray) in the missions at various places grouped and marked. A - Bhaluka, B - Suri, C - Kulti, D - Bolpur, E - Muluk (see Table 1 for details) .

variation in atmospheric radioactivity during different phases of solar activity also has been reported from measurements over Israel (Yaniv et al., 2016), Murmansk (Russia) and Antarctica (Charakhchyan et al., 1975). The result is clearly due to the direct consequence of the regulation of the primary cosmic rays by solar winds.

#### 5.4. Variation of Regener-Pfotzer height

Figure 5 shows the RP-heights obtained in different missions. Except one point from the mission (no. 1) in June, 2012 at latitude  $23.35^\circ$  N all the other RP-heights have their mean at  $15.0 \pm 0.32$  km while the missions took place in the geographic latitude range of  $23.65 - 23.91^\circ$  N. This corresponds to the variation of geomagnetic latitude of  $14.44 - 14.70^\circ$  N. It is possible that due to excess of solar activity in 2012 during solar maximum, the inseparable solar radiation also contributed to CR.

#### 5.5. Effects of solar activity on secondary cosmic rays

To study the effects of solar activity on the atmospheric radiation due to CRs, the radiation count rates at the RP-max in different missions are plotted in Figure 6, along with the sunspot numbers and the 10.7 cm radio flux both with a moving average over previous 10 days. As evident from the Figure the solar parameters show an anti-correlation with the radiation counts at RP-max.

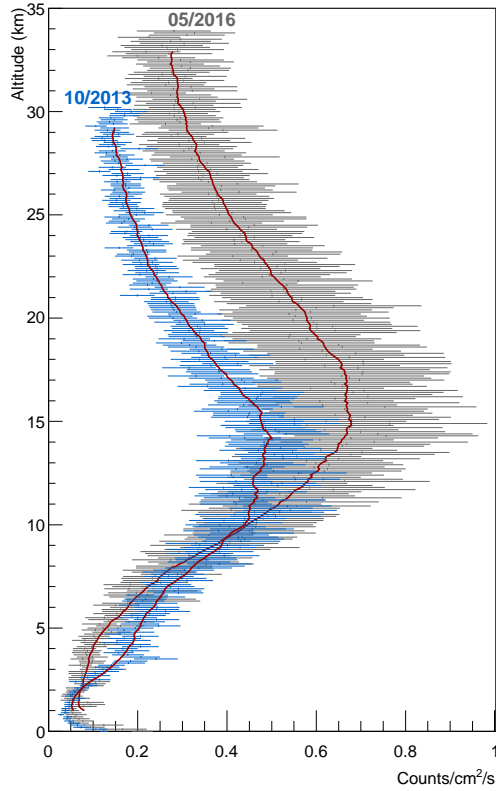


Figure 4: Vertical profile of the secondary cosmic ray counts. Two different data sets from two missions during different phases of solar activity are shown: (blue) October, 2013 when the Sun undergoing maximum activity and (gray) May, 2016 after the solar maxima period.

The correlation between daily sunspot number ( $S$ ) averaged over previous 3 days and radiation count rate ( $C$ ) at the RP-max is shown in Figure 7. The plot is fitted with the straight line:

$$C = 0.793 - 0.0018 S \quad (8)$$

with a reduced  $\chi^2$  value of 6.14/9. This shows a strong anti-correlation with a correlation coefficient of  $-0.84$  and a t-test indicates the anti-correlation is statistically significant at the 95% confidence level.

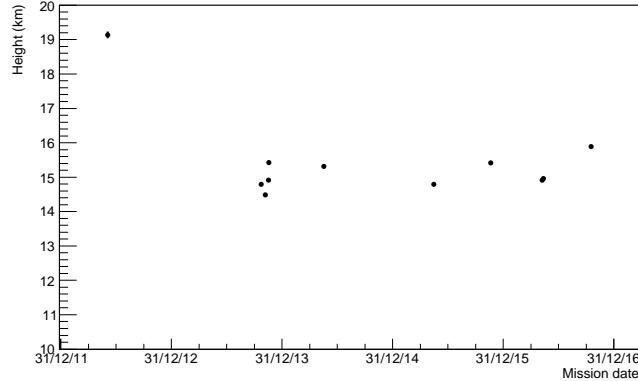


Figure 5: Regener-Pfotzer height obtained for various missions from the secondary cosmic-ray counts variation with altitude.

## 6. Conclusions

A series of unique low cost experiments using light weight scintillator detector on board rubber weather balloons have been conducted to measure the solar effect on the secondary cosmic rays for a time period covering the solar maximum of the 24th solar cycle. Location of these experiments were confined near the Tropic of Cancer to measure these effects, even at relatively low geomagnetic latitude where the rigidity cut-off for the primary cosmic rays is very high. The dependence of the RP-height with the rigidity cut-off match generally well with the trend obtained for the same at other higher latitudes (Bazilevskaya and Svirzevskaya, 1998; Li et al., 2007). Results from the missions at different solar phases, however shows that the RP-height itself does not change significantly with the solar activity. We noticed a significant effect of solar activity on the radiation counts at RP-max. We find that the count rate is anti-correlated with the solar parameters directly related to the solar activity. Li et al. (2007) also reported a slight decrease of the count rate with increasing sunspot number over Hong Kong sky. (Yaniv et al., 2016) found some similar results as reported here from the measurement of vertical ionization profile over southern Israel. They also found significant anti-correlation of ionisation counts with the solar modulation potential presenting the activity of the Sun during the 24th solar cycle. Therefore, the general conclusion of this paper could be taken to be universally true, though the degree may be location dependent.

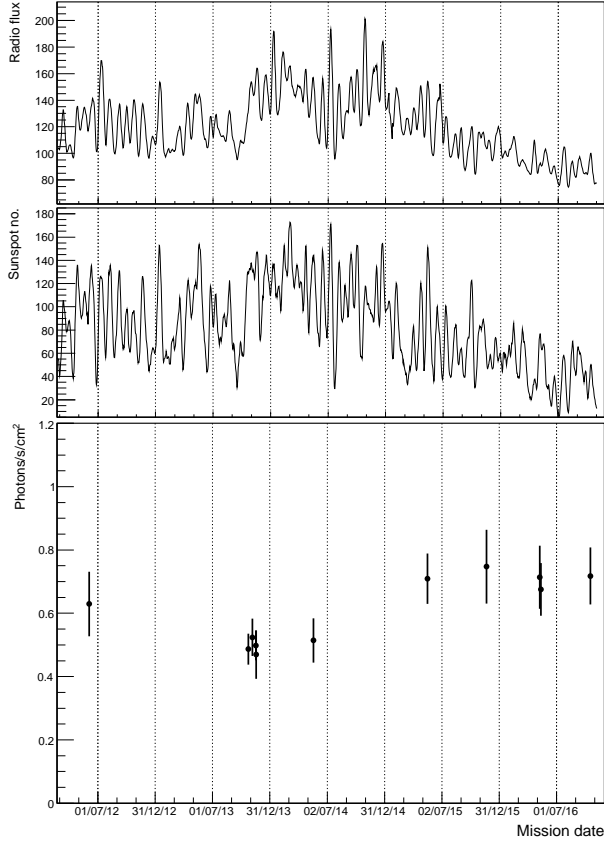


Figure 6: Variation of solar 10.7 cm radio flux (in unit of  $10^{-22} \text{ Watt } m^{-2} Hz^{-1}$ ) and the sunspot numbers (both averaged over previous 10 days) along with CR secondary photon counts at Regener-Pfotzer maximum in different missions.

## Acknowledgments

The authors would like to thank the present and past balloon group team members, such as, Dr. S. Mondal, Mr. S. Chakraborty, Mr. S. Midya, Mr. H. Roy, Mr. R. C. Das and Mr. U. Sardar for their valuable supports at various stages. We also thank Ministry of Earth Sciences (Government of India) for financial supports to some members of the team.

## References

Ageshin P. N., Svirzhevsky N. S., Charakhchyan A. N., Krasotkin A. F. 1981, The latitude measurements of the ionizing and X-ray radiation at

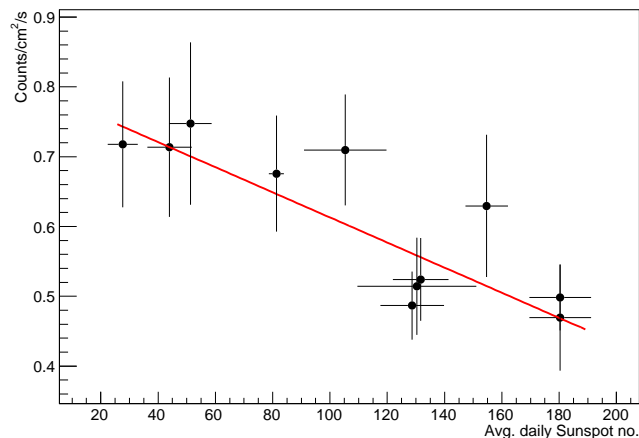


Figure 7: Correlation between the daily sunspot number averaged over previous 3 days and radiation counts at the Regener-Pfotzer maximum.

sea level. Proc. 17th International Cosmic Ray Conference, Paris, France, 1981. Paris: Commissariat a l’Energie Atomique, 1981, 4, 233–236.

Bazilevskaya, G. A., & Svirzevskaya, A. K. 1998, On the stratospheric measurements of cosmic rays, *SpScR* 85, 431–521.

Bazilevskaya, G. A., Krainev, M. B., & Makhmutove, V. S. 2000, Effects of cosmic rays on the Earths environment, *JASTPh* 62, 1577–1586.

Bobik, P., Boella, G., Boschini, M. J., Gervasi, M., Grandi, D., Kudela, K., Pensotti, S., & Rancoita, P. G. 2006, Magnetospheric transmission function approach to disentangle primary from secondary cosmic ray fluxes in the penumbra region, *JGRA* 111, 5205.

Chakrabarti, S. K., Bhowmick, D., Chakraborty, S., Palit, S., Mondal, S. K., Bhattacharya, A., Midya, S., & Chakrabarti, S. 2014, Study of properties of cosmic rays and solar X-ray flares by balloon borne experiments, *IJP* 88, 333–341.

Chakrabarti, S. K., Sarkar, R., Bhowmick, D., & Bhattacharya, A., 2017, Study of high energy phenomena from near space using low-cost meteorological balloons, *Exp. Astrn.*, 43(3), 311-338.

- Charakhchyan A. N., Bazilevskaya G. A., Stozhkov Yu. I., Charakhchyan T. N. 1975, Investigation of the long-term variations of cosmic ray latitude effect in the Earth atmosphere. Proc. 14th ICRC, Munchen, 1975, 3, 1020–1024.
- Charakhchyan A. N., Ageshin P. N., Bazilevskaya G. A., Golenkov A. E., Krasotkin A. F., Svirzhevsky N. S., Stozhkov Yu. I., Charakhchyan T. N. 1979, Measurements of ionizing radiation at sea level in various geographic latitudes and in Antarctica. Proc. 16th ICRC, Kyoto, 1979, 4, 253–257.
- Dorman, L. I., Smirnov, V. S., & Tyasto, M. I. 1971, Cosmic rays in the Earths magnetic field, Nauka, Moscow.
- Gaisser, T. K. 1990, Cosmic Rays and Particle Physics, Cambridge University Press.
- Geomagsphere.org, 2016, <http://www.geomagsphere.org>. Accessed 20 Aug. 2016.
- Golenkov A. E., Okhlopov V. P., Svirzhevsky N. S., Svirzhevskaya A. K., Stozhkov Yu. I. 1977, Latitude measurements of cosmic ray intensity in the stratosphere during the solar minimum in 1975-1976. Proc. 15th ICRC, Plovdiv, 1977, 4, 229–233.
- Golenkov A. E., Svirzhevskaya A. K., Svirzhevsky N. S., Stozhkov Yu. I. 1990, Cosmic ray latitude survey in the stratosphere during the 1987 solar minimum. Proc. 21st ICRC, Adelaide, 1990, 7, 14–17.
- Grieder, P. K. F. 2001, Cosmic Rays at Earth: Researcher’s Reference Manual and Data Book, Elsevier Science.
- Harrison, R. G., Nicoll, K. A., Aplin, K. L. 2014, Vertical profile measurements of lower troposphere ionisation, JASTP, 119, 203–210.
- Hatakka, J., Paatero, J., Kyro, E., Antikainen, V., & Viisanen, Y. 2000, Monitoring of radioactivity in the upper atmosphere with radiosoundings, Proceedings of Symposium on Nuclear, Biological and Chemical Threats in the 21st Century (NBC2000), June 13–15, 2000, Helsinki University of Technology, Espo, Finland, pp. 269–270.



- Li, S. W., Li, Y. S., & Tsui, K. C. 2007, Radioactivity in the atmosphere over Hong Kong, *JEnRa* 94, 98–106.
- Miroshnichenko, L. I. 2003, Radiation hazard in space, Springer-Science+Business Media.
- Nicoll, K. A. 2012, Measurements of Atmospheric Electricity Aloft, *SGeo*, 33, 991–1057.
- Pfotzer, G. 1936, Dreifachkoinzidenzen der Ultrastrahlung aus vertikaler Richtung in der Stratosphere (in German), *Z. Phys.* 102, 23–58.
- Radiation exposure prediction, 2016, <http://csp.res.in/ICSP-WEB/xrayfiles/xray.html>. Accessed 28 Aug. 2016.
- Regener, E. 1933, New Results in Cosmic Ray Measurements, *Nature*, 132, 696–698.
- Regener, E. and Pfotzer, G. 1935, Intensity of the Cosmic Ultra-Radiation in the Stratosphere with the Tube-Counter, *Nature*, 134, 325–325.
- Saint-Gobain Crystals, 2016, <http://www.crystals.saint-gobain.com>. Accessed 28 Aug. 2016.
- Shea M. A., Smart D. F., Stozhkov Yu. I., Svirzhevsky N. S., Svirzhevskaya A. K., Bazilevskaya G. A., Charakhchyan T. N. 1987, Cosmic ray latitude surveys in the Atlantic ocean area. *Proc. 20th ICRC*, Moscow, 1987, 4, 201–203.
- Shönfelder, V., Graser, U., & Daugherty, J. 1977, Diffuse cosmic and atmospheric MeV gamma radiation from balloon observations, *ApJ* 217, 306–319.
- Störmer, C. 1955, *The polar aurora*, Oxford University Press, New York.
- Yaniv, R., Yair, Y., Price, C., Nicoll, K., Harrison, G., Artamonov, A., Usoskin, I. 2016, Balloon measurements of the vertical ionization profile over southern Israel and comparison to mid-latitude observations, *JASTP*, 149, 87–92.